

# Acoustic scaling of anisotropic flow in shape-engineered events: implications for extraction of the specific shear viscosity of the quark gluon plasma

Roy A. Lacey,<sup>1,2,\*</sup> D. Reynolds,<sup>1</sup> A. Taranenko,<sup>1</sup> N. N. Ajitanand,<sup>1</sup>  
J. M. Alexander,<sup>1</sup> Fu-Hu Liu,<sup>1,3</sup> Yi Gu,<sup>1</sup> and A. Mwai<sup>1</sup>

<sup>1</sup>*Department of Chemistry, Stony Brook University,  
Stony Brook, NY, 11794-3400, USA*

<sup>2</sup>*Department of Physics and Astronomy, Stony Brook University,  
Stony Brook, NY, 11794-3800*

<sup>3</sup>*Institute of Theoretical Physics, Shanxi University,  
Taiyuan, Shanxi 030006, China*

(Dated: July 30, 2018)

It is shown that the acoustic scaling patterns of anisotropic flow for different event shapes at a fixed collision centrality (shape-engineered events), provide robust constraints for the event-by-event fluctuations in the initial-state density distribution from ultrarelativistic heavy ion collisions. The empirical scaling parameters also provide a dual-path method for extracting the specific shear viscosity  $(\eta/s)_{\text{QGP}}$  of the quark-gluon plasma (QGP) produced in these collisions. A calibration of these scaling parameters via detailed viscous hydrodynamical model calculations, gives  $(\eta/s)_{\text{QGP}}$  estimates for the plasma produced in collisions of Au+Au ( $\sqrt{s_{\text{NN}}} = 0.2$  TeV) and Pb+Pb ( $\sqrt{s_{\text{NN}}} = 2.76$  TeV). The estimates are insensitive to the initial-state geometry models considered.

PACS numbers: 25.75.-q, 12.38.Mh, 25.75.Ld, 24.10.Nz

Considerable attention has been given to the study of anisotropic flow measurements in heavy-ion collisions at both the Relativistic Heavy Ion Collider (RHIC) and the Large Hadron Collider (LHC) [1–14]. Recently, the attack has focused on studies of initial state fluctuations and their role in the extraction of the specific shear viscosity (i.e. the ratio of shear viscosity to entropy density  $\eta/s$ ) of the quark-gluon plasma (QGP). These flow measurements are routinely quantified as a function of collision centrality (cent) and particle transverse momentum  $p_{\text{T}}$  by the Fourier coefficients  $v_n$

$$v_n(p_{\text{T}}, \text{cent}) = \langle \cos[n(\phi - \Psi_n)] \rangle. \quad (1)$$

Here  $\phi$  is the azimuthal angle of an emitted particle and  $\Psi_n$  is the estimated azimuth of the  $n$ -th order event plane [15, 16]; brackets denote averaging over particles and events. The current measurements for charged hadrons [17, 18] indicate significant odd and even  $v_n$  coefficients up to about the sixth harmonic.

The estimates of  $(\eta/s)_{\text{QGP}}$  from these  $v_n$  measurements have indicated a small value (i.e. 1-3 times the lower conjectured bound of  $1/4\pi$  [19]). Substantial theoretical uncertainties have been assigned primarily to incomplete knowledge of the initial-state geometry and its associated event-by-event fluctuations. Indeed, an uncertainty of  $\mathcal{O}(100\%)$  in the value of  $(\eta/s)_{\text{QGP}}$  extracted from  $v_2$  measurements at RHIC ( $\sqrt{s_{\text{NN}}} = 0.2$  TeV) [5, 6], has been attributed to a  $\sim 20\%$  uncertainty in the theoretical estimates [20, 21] for the event-averaged initial eccentricity  $\varepsilon_2$  of the collision zone. Here, it is important to note that a robust method of extraction should not depend on the initial geometrical conditions since  $(\eta/s)_{\text{QGP}}$  is only a property of the medium itself.

Recent attempts to reduce the uncertainty for  $(\eta/s)_{\text{QGP}}$  have focused on: (i) the development of a more constrained description of the fluctuating initial-state geometry [22], (ii) the combined analysis of  $v_2$  and  $v_3$  [18, 23, 24] and other higher order harmonics [11] and (iii) a search for new constraints via “acoustic scaling” of  $v_n$  [25–27]. The latter two approaches [(ii) and (iii)] utilize the prediction that the strength of the dissipative effects which influence the magnitude of  $v_n(\text{cent})$ , grow exponentially as  $n^2$  and  $1/\bar{R}$  [25, 26, 28];

$$\frac{v_n(\text{cent})}{\varepsilon_n(\text{cent})} \propto \exp\left(-\beta \frac{n^2}{\bar{R}}\right), \quad \beta \sim \frac{4}{3} \frac{\eta}{Ts}, \quad (2)$$

where  $\varepsilon_n$  is the  $n$ -th order eccentricity moment,  $T$  is the temperature and  $\bar{R}$  is the initial-state transverse size of the collision zone. Thus, a characteristic linear dependence of  $\ln(v_n/\varepsilon_n)$  on  $n^2$  and  $1/\bar{R}$  [cf. Eq. 2], with slopes  $\beta' \propto (\eta/s)_{\text{QGP}}$  and  $\beta'' \propto (\eta/s)_{\text{QGP}}$  are to be expected.

These scaling patterns have indeed been validated and shown to give important constraints for the extraction of  $(\eta/s)_{\text{QGP}}$  from both RHIC ( $\sqrt{s_{\text{NN}}} = 0.2$  TeV) and LHC ( $\sqrt{s_{\text{NN}}} = 2.76$  TeV) data [25, 26]. Here, we explore a more explicit constraint for initial-state shape fluctuations, via scaling studies of  $v_n$  measurements obtained for shape-engineered events, i.e. different event shapes at a fixed centrality.

Such a constraint is derived from the expectation that the event-by-event fluctuations in anisotropic flow, result primarily from fluctuations in the size and shape (eccentricity) of the initial-state density distribution. Thus, various cuts on the full distribution of initial shapes [at a given centrality], should result in changes in the magnitudes of  $\langle \varepsilon_n \rangle$ ,  $\langle \bar{R}_n \rangle$  and  $\langle v_n \rangle$ . Note however, that acceptable models for the initial-state fluctuations should

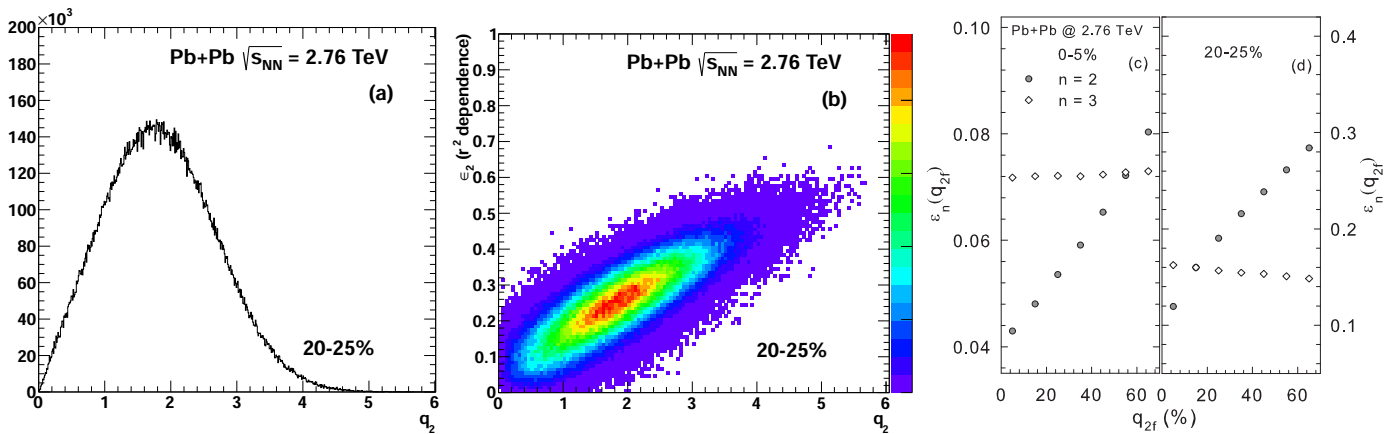


FIG. 1. (Color online) Calculated values for (a) the  $q_2$  distribution for 20-25% central events; (b)  $\varepsilon_2$  vs.  $q_2$  for 20-25% central events; (c)  $\varepsilon_{2,3}$  vs.  $q_{2f}$  for 0-5% central events; (d)  $\varepsilon_{2,3}$  vs.  $q_{2f}$  for 20-25% central events. The calculations were made for Pb+Pb collisions at  $\sqrt{s_{NN}} = 2.76$  TeV with the MC-Glauber model.

76 give  $\langle \varepsilon_n \rangle$  and  $\langle \bar{R}_n \rangle$  values each of which lead to acoustic  
 77 scaling of  $\langle v_n \rangle$  with little, if any, change in the slope pa-  
 78 rameter  $\beta'$  ( $\beta''$ ) for different event shape selections, i.e.,  
 79  $\beta'$  ( $\beta''$ )  $\propto (\eta/s)_{QGP}$  is a property of the medium, not the  
 80 initial state geometry.

81 The  $q_n$  flow vector has been proposed [29] as a tool  
 82 to select different initial shapes from the distribution of  
 83 initial-state geometries at a fixed centrality;

$$Q_{n,x} = \sum_i^M \cos(n\phi_i); \quad Q_{n,y} = \sum_i^M \sin(n\phi_i); \quad (3)$$

$$q_n = Q_n / \sqrt{M}, \quad (4)$$

84 where  $M$  is the particle multiplicity and  $\phi_i$  are the az-  
 85 imuthal angles of the particles in the sub-event used to  
 86 determine  $q_n$ . We use this technique for model-based  
 87 evaluations of  $\varepsilon_2(q_2, \text{cent})$  and  $\bar{R}(q_2, \text{cent})$  to perform val-  
 88 idation tests for acoustic scaling of recent  $v_2(q_2, \text{cent})$   
 89 measurements, as well as to determine if  $\beta''$  is indepen-  
 90 dent of event shape. We use the acoustic scaling patterns,  
 91 indicated in the results of  $q_n$ -averaged viscous hydro-  
 92 dynamical calculations [30], to calibrate  $\beta'$  and  $\beta''$  and  
 93 make estimates of  $(\eta/s)_{QGP}$  for the plasma produced in  
 94 Au+Au and Pb+Pb collisions at RHIC and the LHC re-  
 95 spectively.

96 The data employed in this work are taken from mea-  
 97 surements by the ALICE and CMS collaborations for  
 98 Pb+Pb collisions at  $\sqrt{s_{NN}} = 2.76$  TeV [31, 32], as well  
 99 as measurements by the STAR collaboration for Au+Au  
 100 collisions at  $\sqrt{s_{NN}} = 200$  GeV [7, 33]. The ALICE  
 101 measurements [31] exploit a three subevents technique  
 102 to evaluate  $v_2(q_2, \text{cent})$ , where the first subevent  $SE_1$  is  
 103 used to determine  $q_2$ , and the particles in the second  
 104 subevent  $SE_2$  are used to evaluate  $v_2(q_2, \text{cent})$  relative to  
 105 the  $\Psi_2$  event plane determined from the particles in the  
 106 third subevent  $SE_3$ . To suppress non-flow correlations,  
 107 the detector subsystems used to select  $SE_{1,2,3}$  were cho-

108 sen so as to give a sizable pseudo-rapidity gap ( $\Delta\eta_p$ )  
 109 between the particles in different subevents. For each  
 110 centrality,  $v_2(q_2)$  measurements were made for the full  $q_2$   
 111 distribution [ $v_2(q_{2(\text{Avg.})})$ ], as well as for events with the  
 112 10% lowest [ $v_2(q_{2(\text{Lo})})$ ] and 5% highest [ $v_2(q_{2(\text{Hi})})$ ] values  
 113 of the  $q_2$  distribution.

114 The CMS [30] and STAR [33]  $v_n(\text{cent})$  measurements  
 115 for  $n = 2 - 6$  (CMS) and  $n = 2$  (STAR) were selected  
 116 to ensure compatibility with the viscous hydrodynamical  
 117 calculations discussed below. An explicit selection on  
 118  $q_n$  was not used for these measurements; instead, they  
 119 were averaged over the respective  $q_n$  distributions to give  
 120  $v_n(q_{n(\text{Avg.})}, \text{cent}) \equiv v_n(\text{cent})$ . The systematic errors for  
 121 the ALICE, CMS and STAR measurements are reported  
 122 in Refs. [31], [32] and [33] respectively.

123 Monte Carlo versions were used for (a) the Glauber  
 124 (MC-Glauber) [34] and (b) Kharzeev-Levin-Nardi [21,  
 125 35, 36] (MC-KLN) models for fluctuating initial condi-  
 126 tions. Each was used to compute the number of partic-  
 127 ipants  $N_{\text{part}}(\text{cent})$ ,  $q_n(\text{cent})$ ,  $\varepsilon_n(\text{cent})$  [with weight  
 128  $\omega(\mathbf{r}_\perp) = \mathbf{r}_\perp^n$ ] and  $\bar{R}_n(\text{cent})$  from the two-dimensional  
 129 profile of the density of sources in the transverse plane  
 130  $\rho_s(\mathbf{r}_\perp)$  [23], where  $1/\bar{R}_2 = \sqrt{(1/\sigma_x^2 + 1/\sigma_y^2)}$ , with  $\sigma_x$   
 131 and  $\sigma_y$  the respective root-mean-square widths of the  
 132 density distributions. Computations for these initial-  
 133 state geometric quantities were also made for 5% and  
 134 10% increments in  $q_n$ , from the lowest ( $q_{n(\text{Lo})}$ ) to the  
 135 highest ( $q_{n(\text{Hi})}$ ) values of the  $q_n$  distribution. The com-  
 136 putations were performed for both Au+Au ( $\sqrt{s_{NN}} = 0.2$   
 137 TeV) and Pb+Pb ( $\sqrt{s_{NN}} = 2.76$  TeV) collisions. From  
 138 variations of the MC-Glauber and MC-KLN model pa-  
 139 rameters, a systematic uncertainty of 2-3% was obtained  
 140 for  $\bar{R}$  and  $\varepsilon$  (respectively).

142 Figure 1(a) shows a representative  $q_2$  distribution for  
 143 20-25% central MC-Glauber events for Pb+Pb collisions.  
 144 The relatively broad distribution reflects the effects of

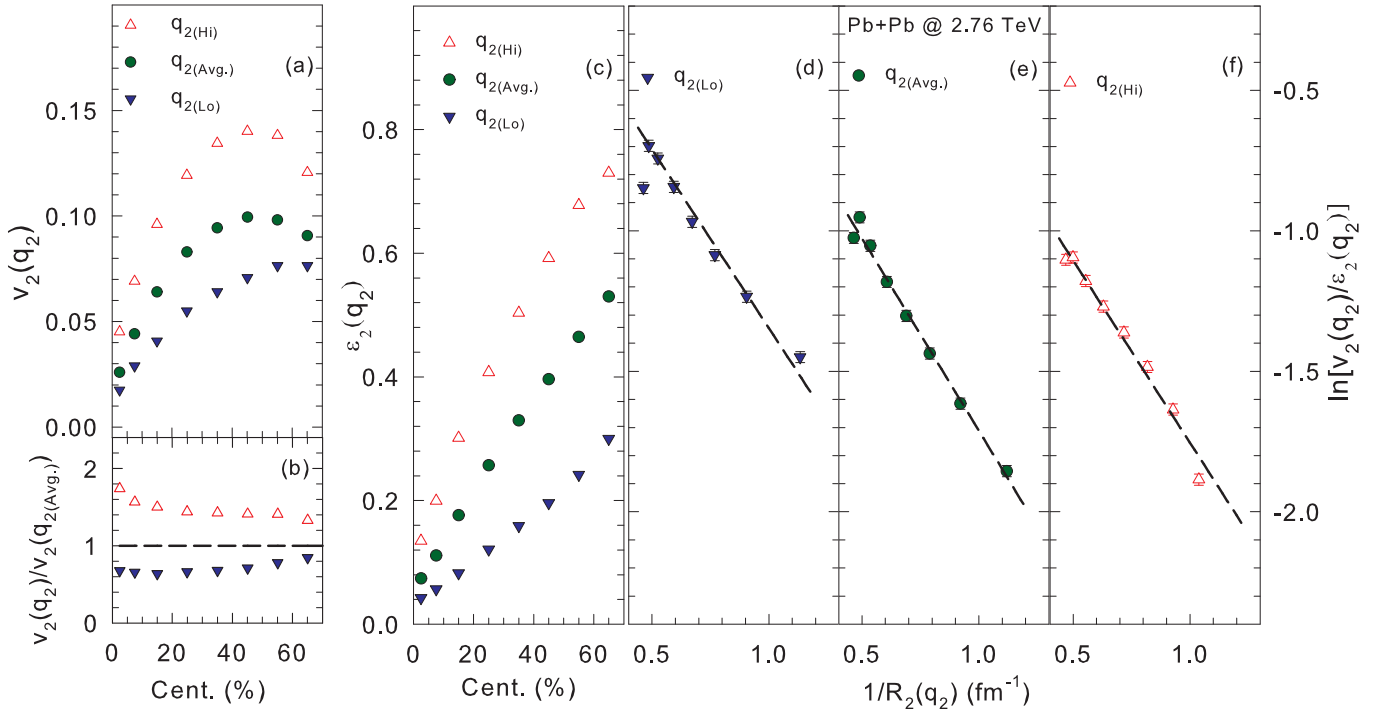


FIG. 2. (a) (Color online) Centrality dependence of  $v_2(q_{2(\text{Lo})})$ ,  $v_2(q_{2(\text{Avg.})})$  and  $v_2(q_{2(\text{Hi})})$  [31] for  $0 < \text{cent} < 70\%$  for Pb+Pb collisions at  $\sqrt{s_{\text{NN}}} = 2.76$  TeV. (b) Centrality dependence of the ratios  $v_2(q_{2(\text{Lo})})/v_2(q_{2(\text{Avg.})})$  and  $v_2(q_{2(\text{Hi})})/v_2(q_{2(\text{Avg.})})$ . (c) Centrality dependence of  $\varepsilon_2(q_{2(\text{Lo})})$ ,  $\varepsilon_2(q_{2(\text{Avg.})})$  and  $\varepsilon_2(q_{2(\text{Hi})})$ , evaluated with the MC-Glauber model. (d)  $\ln[v_2(q_2)/\varepsilon_2(q_2)]$  vs.  $1/\bar{R}_2(q_2)$  for  $q_{2(\text{Lo})}$ . (e) same as (d) but for  $q_{2(\text{Avg.})}$ . (f) same as (d) but for  $q_{2(\text{Hi})}$ .

145 sizable event-by-event fluctuations convoluted with sta- 172  
 146 tistical fluctuations due to finite particle number. Quali- 173  
 147 tatively similar distributions were obtained for other cen- 174  
 148 tralities and for other harmonics. These  $q_n$  distributions 175  
 149 were partitioned into the 5% and 10% increments  $q_{nf}$  176  
 150 [from the lowest to the highest values] and used for fur- 177  
 151 ther detailed selections on the event shape. 178

152 The effectiveness of such selections is illustrated in 179  
 153 Fig. 1(b), which shows a strong correlation between  $\varepsilon_2$  180  
 154 and  $q_2$  for 20-25% central Pb+Pb events. Similar trends 181  
 155 were obtained for other centrality cuts and for other har- 182  
 156 monics. Figs. 1(c) and (d) show the dependence of  $\varepsilon_2$  and 183  
 157  $\varepsilon_3$  on  $q_{2f}$  for two centrality selections as indicated. For 184  
 158 central collisions (0-5%),  $\varepsilon_2(q_{2f})$  and  $\varepsilon_3(q_{2f})$  both show 185  
 159 an increase with  $q_{2f}$ , albeit with a much stronger depen- 186  
 160 dence for  $\varepsilon_2(q_{2f})$ . This increase is expected to lead to a 187  
 161 corresponding increase of  $v_2(q_{2f})$  and  $v_3(q_{2f})$  with  $q_{2f}$ . 188

162 Fig. 1(d) indicates a similar increase of  $\varepsilon_2(q_{2f})$  with  $q_{2f}$  189  
 163 for 20-25% central collisions. However,  $\varepsilon_3(q_{2f})$  indicates 190  
 164 a decrease with  $q_{2f}$ , suggesting that a characteristic in- 191  
 165 version of the dependence of  $v_3(q_2)$  is to be expected as a 192  
 166 signature in future  $v_3(q_2)$  measurements for central and 193  
 167 mid-central collisions. 194

168 Figure 2(a) shows the centrality dependence for one set 195  
 169 of the shape-engineered measurements of  $v_2(q_{2(\text{Lo})}, \text{cent})$ , 196  
 170  $v_2(q_{2(\text{Avg.})}, \text{cent})$  and  $v_2(q_{2(\text{Hi})}, \text{cent})$  reported in Ref. [31]. 197  
 171 They show that this event-shape selection leads to lower 198

(higher) values of  $v_2(q_2, \text{cent})$  for  $q_2$  values lower (higher) 172  
 than  $q_{2(\text{Avg.})}$ . They also show that such selections 173  
 can lead to a sizable difference (more than a factor of 174  
 two) between  $v_2(q_{2(\text{Hi})}, \text{cent})$  and  $v_2(q_{2(\text{Lo})}, \text{cent})$ , as il- 175  
 lustrated in Fig. 2(b). Strikingly similar differences 176  
 can be observed in Fig. 2(c) for the MC-Glauber re- 177  
 sults shown for  $\varepsilon_2(q_{2(\text{Lo})}, \text{cent})$ ,  $\varepsilon_2(q_{2(\text{Avg.})}, \text{cent})$  and 178  
 $\varepsilon_2(q_{2(\text{Hi})}, \text{cent})$ . They suggest that differences in the mea- 179  
 sured magnitudes for  $v_2(q_{2(\text{Lo})}, \text{cent})$ ,  $v_2(q_{2(\text{Avg.})}, \text{cent})$  180  
 and  $v_2(q_{2(\text{Hi})}, \text{cent})$ , are driven by the corresponding dif- 181  
 ferences in the calculated magnitudes for  $\varepsilon_2(q_{2(\text{Lo})}, \text{cent})$ , 182  
 $\varepsilon_2(q_{2(\text{Avg.})}, \text{cent})$  and  $\varepsilon_2(q_{2(\text{Hi})}, \text{cent})$ . 183

The shape-selected measurements in Fig. 2(a) for 184  
 $v_2(q_{2(\text{Lo})}, \text{cent})$ ,  $v_2(q_{2(\text{Avg.})}, \text{cent})$  and  $v_2(q_{2(\text{Hi})}, \text{cent})$  all 185  
 show an increase from central to mid-central colli- 186  
 sions, as would be expected from an increase in 187  
 $\varepsilon_2(q_{2(\text{Lo})}, \text{cent})$ ,  $\varepsilon_2(q_{2(\text{Avg.})}, \text{cent})$  and  $\varepsilon_2(q_{2(\text{Hi})}, \text{cent})$  over 188  
 the same centrality range [cf. Fig. 2(c)]. For  $\text{cent} \gtrsim$  189  
 45% however, the decreasing trends for  $v_2(q_{2(\text{Lo})}, \text{cent})$ , 190  
 $v_2(q_{2(\text{Avg.})}, \text{cent})$  and  $v_2(q_{2(\text{Hi})}, \text{cent})$  contrasts with the 191  
 increasing trends for  $\varepsilon_2(q_{2(\text{Lo})}, \text{cent})$ ,  $\varepsilon_2(q_{2(\text{Avg.})}, \text{cent})$  192  
 and  $\varepsilon_2(q_{2(\text{Hi})}, \text{cent})$ , suggesting that the viscous effects 193  
 due to the smaller systems produced in peripheral colli- 194  
 sions, serve to suppress  $v_2(q_{2(\text{Lo})}, \text{cent})$ ,  $v_2(q_{2(\text{Avg.})}, \text{cent})$  195  
 and  $v_2(q_{2(\text{Hi})}, \text{cent})$ . This is confirmed by the symbols 196  
 and dashed curves in Figs. 2(d) - (f) which validates 197  
 the expected linear dependence of  $\ln[v_2(q_2)/\varepsilon_2(q_2)]$  on 198

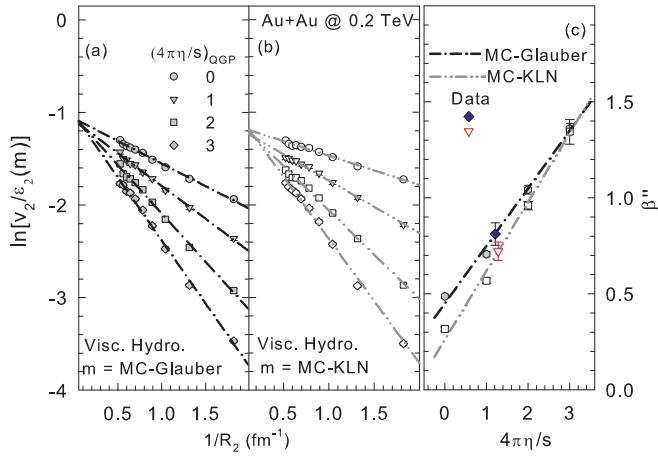


FIG. 3. (Color online)  $\ln[v_2/\varepsilon_2]$  vs.  $1/\bar{R}_2$  for viscous hydrodynamical calculations [30] for Au+Au collisions at  $\sqrt{s_{NN}} = 0.2$  TeV with (a) MC-Glauber initial-state geometries and (b) MC-KLN initial-state geometries; the dashed-dot and the dotted-dashed curves represent linear fits. Results are shown for several values of  $4\pi\eta/s$  as indicated. (c) Calibration curve for  $\beta''$  vs.  $4\pi\eta/s$ ; the  $\beta''$  values are obtained from the slopes of the curves shown in (a) and (b). The indicated data points are obtained from a linear fit to  $\ln[v_2/\varepsilon_2]$  vs.  $1/\bar{R}_2$  for the STAR Au+Au data at  $\sqrt{s_{NN}} = 0.2$  TeV [7, 33]

199  $1/\bar{R}_2(q_2)$  (cf. Eq. 2) for the data shown in Fig. 2(a).  
 200 The dashed curves, which indicate a similar slope value  
 201 ( $\beta'' \sim 1.3 \pm 0.07$ ) for each of the scaling curves in  
 202 Figs. 2(d) - (f), provide an invaluable model constraint  
 203 for the event-by-event fluctuations in the initial-state  
 204 density distribution, as well as for robust estimates of  
 205  $\eta/s$ .

207 The acoustic scaling patterns summarized in Eq. 2 are  
 208 also exhibited in the results of  $q_n$ -averaged viscous hydro-  
 209 dynamical calculations [30] as demonstrated in Figs. 3(a)  
 210 and (b) and Fig. 4(a). The scaled results, which are  
 211 shown for several values of  $4\pi\eta/s$  in each case, exhibit  
 212 the expected linear dependence of  $\ln(v_n/\varepsilon_n)$  on  $1/\bar{R}$  for  
 213 both MC-Glauber (Figs. 3(a)) and MC-KLN (Figs. 3(b))  
 214 initial conditions, as well as the expected linear depen-  
 215 dence of  $\ln(v_n/\varepsilon_n)$  on  $n^2$  (Fig. 4(a)). They also give a  
 216 clear indication that the slopes of these curves are sensi-  
 217 tive to the magnitude of  $4\pi\eta/s$ . Therefore, we use them  
 218 to calibrate  $\beta''$  and  $\beta'$  to obtain estimates for  $(4\pi\eta/s)_{\text{QGP}}$   
 219 for the plasma produced in RHIC and LHC collisions.

220 Figure 3(c) shows the calibration curves for  $\beta''$  vs.  
 221  $4\pi\eta/s$ , obtained from the viscous hydrodynamical calcu-  
 222 lations shown in Figs. 3(a) and (b). The filled circles and  
 223 the associated dot-dashed curve, represent the slope param-  
 224 eters ( $\beta''$ ) obtained from linear fits to the viscous hydro-  
 225 dynamical results for MC-Glauber initial conditions  
 226 shown in Fig. 3(a). The open squares and the associated  
 227 dot-dot-dashed curve, represent the slope parameters ob-  
 228 tained from linear fits to the viscous hydrodynamical re-  
 229 sults for MC-KLN initial conditions shown in Fig. 3(b).

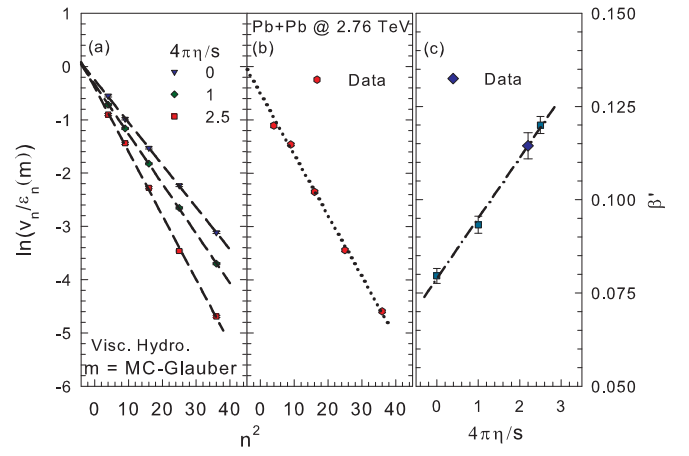


FIG. 4. (Color online) (a)  $\ln(v_n/\varepsilon_n)$  vs.  $n^2$  from viscous hydrodynamical calculations [30] for three values of specific shear viscosity as indicated. (b)  $\ln(v_n/\varepsilon_n)$  vs.  $n^2$  for Pb+Pb data. The  $p_T$ -integrated  $v_n$  results in (a) and (b) are for 0.2% central Pb+Pb collisions at  $\sqrt{s_{NN}} = 2.76$  TeV [30]; the curves are linear fits. (c) Calibration curve for  $\beta'$  vs.  $4\pi\eta/s$ ; the  $\beta'$  values are obtained from the slopes of the curves shown in (a). The indicated data point is obtained from a linear fit to the scaled data shown in (b).

230 The STAR  $v_2(\text{cent})$  data for Au+Au collisions, also show  
 231 the expected linear dependence of  $\ln(v_2/\varepsilon_2)$  on  $1/\bar{R}_2$  for  
 232  $\varepsilon_2$  and  $\bar{R}_2$  values obtained from the MC-Glauber and  
 233 MC-KLN models respectively. The filled diamond and  
 234 the open triangle in Fig. 3(c), represent the slopes ex-  
 235 tracted from the respective scaling plots for MC-Glauber  
 236 and MC-KLN initial conditions; a comparison to the re-  
 237 spective calibration curves in Fig. 3(c), gives the estimate  
 238  $\langle 4\pi\eta/s \rangle_{\text{QGP}} \sim 1.3 \pm 0.2$  for the plasma created in RHIC  
 239 collisions. Here, it is noteworthy that our extraction pro-  
 240 cedure leads to an estimate which is basically insensitive  
 241 to the choice of the MC-Glauber or MC-KLN initial-state  
 242 geometry.

244 The solid squares and the associated dashed-dot curve  
 245 in Fig. 4(c), represent the calibration curve for  $\beta'$  vs.  
 246  $4\pi\eta/s$ , obtained from the linear fits (dashed curves)  
 247 to the viscous hydrodynamical calculations shown in  
 248 Fig. 4(a). Fig. 4(b) shows the expected linear depen-  
 249 dence of  $\ln(v_n/\varepsilon_n)$  on  $n^2$  for CMS Pb+Pb data [30] scaled  
 250 with same  $\varepsilon_n$  values employed in Fig. 4(a). The slope  
 251 extracted from Fig. 4(b) is indicated by the solid blue  
 252 diamond shown in Fig. 4(c); a comparison with the the  
 253 calibration curve gives the the estimate  $\langle 4\pi\eta/s \rangle_{\text{QGP}} \sim$   
 254  $2.2 \pm 0.2$  for the plasma created in LHC collisions.

255 The  $\langle 4\pi\eta/s \rangle_{\text{QGP}}$  estimates for the plasma produced  
 256 in RHIC and LHC collisions are in reasonable agreement  
 257 with recent  $\langle \eta/s \rangle$  estimates [11, 26, 36–38]. While further  
 258 calculations will undoubtedly be required to reduce pos-  
 259 sible model-driven calibration uncertainties, our method  
 260 benefits from the implicit constraint for the event-by-  
 261 event fluctuations in the initial-state density distribution,

as well as its lack of sensitivity to the initial-state models employed in our analysis.

In summary, we have presented a detailed phenomenological exploration of a new constraint for initial-state fluctuations, via scaling studies of  $v_2$  measurements obtained for shape-engineered events. We find acoustic scaling patterns for shape-selected events (via  $q_{2(\text{Lo})}$ ,  $q_{2(\text{Avg.})}$  and  $q_{2(\text{Hi})}$ ) which provide robust constraints for the event-by-event fluctuations in the initial-state density distribution, as well as methodology with two consistent paths for estimating  $(\eta/s)_{\text{QGP}}$  of the QGP produced in Au+Au and Pb+Pb collisions at RHIC and the LHC. A calibration of the method with  $q_2$ -averaged viscous hydrodynamical model calculations, gives estimates for  $(4\pi\eta/s)_{\text{QGP}}$  of  $1.3 \pm 0.2$  and  $2.2 \pm 0.2$ , for the plasma produced in Au+Au ( $\sqrt{s_{NN}} = 0.2$  TeV) and Pb+Pb ( $\sqrt{s_{NN}} = 2.76$  TeV) collisions (respectively). These values are insensitive to the initial-state geometry models employed.

**Acknowledgments** This research is supported by the US DOE under contract DE-FG02-87ER40331.A008.

\* E-mail: Roy.Lacey@Stonybrook.edu

- [1] D. Teaney, Phys.Rev. **C68**, 034913 (2003), arXiv:nucl-th/0301099 [nucl-th].
- [2] R. A. Lacey and A. Taranenko, PoS **CFRNC2006**, 021 (2006), arXiv:nucl-ex/0610029 [nucl-ex].
- [3] R. A. Lacey, N. Ajitanand, J. Alexander, P. Chung, W. Holzmann, et al., Phys.Rev.Lett. **98**, 092301 (2007), arXiv:nucl-ex/0609025 [nucl-ex]; A. Adare et al. (PHENIX Collaboration), Phys.Rev.Lett. **98**, 172301 (2007), arXiv:nucl-ex/0611018 [nucl-ex]; H.-J. Drescher, A. Dumitru, C. Gombeaud, and J.-Y. Ollitrault, Phys.Rev. **C76**, 024905 (2007), arXiv:0704.3553 [nucl-th]; K. Dusling and D. Teaney, Phys.Rev. **C77**, 034905 (2008), arXiv:0710.5932 [nucl-th]; Z. Xu, C. Greiner, and H. Stocker, Phys.Rev.Lett. **101**, 082302 (2008), arXiv:0711.0961 [nucl-th]; D. Molnar and P. Huovinen, J.Phys. **G35**, 104125 (2008), arXiv:0806.1367 [nucl-th]; R. A. Lacey, A. Taranenko, and R. Wei, (2009), arXiv:0905.4368 [nucl-ex]; K. Dusling, G. D. Moore, and D. Teaney, Phys.Rev. **C81**, 034907 (2010), arXiv:0909.0754 [nucl-th]; A. Chaudhuri, J.Phys. **G37**, 075011 (2010), arXiv:0910.0979 [nucl-th]; R. A. Lacey, A. Taranenko, R. Wei, N. Ajitanand, J. Alexander, et al., Phys.Rev. **C82**, 034910 (2010), arXiv:1005.4979 [nucl-ex].
- [4] P. Romatschke and U. Romatschke, Phys.Rev.Lett. **99**, 172301 (2007), arXiv:0706.1522 [nucl-th].
- [5] M. Luzum and P. Romatschke, Phys.Rev. **C78**, 034915 (2008), arXiv:0804.4015 [nucl-th]; Phys.Rev.Lett. **103**, 262302 (2009), arXiv:0901.4588 [nucl-th].
- [6] H. Song, S. A. Bass, U. Heinz, T. Hirano, and C. Shen, Phys.Rev.Lett. **106**, 192301 (2011), arXiv:1011.2783 [nucl-th].
- [7] K. Aamodt et al. (ALICE Collaboration), Phys.Rev.Lett. **105**, 252302 (2010), arXiv:1011.3914 [nucl-ex]; M. Luzum, Phys.Rev. **C83**, 044911 (2011), arXiv:1011.5173 [nucl-th].
- [8] R. A. Lacey, A. Taranenko, N. Ajitanand, and J. Alexander, Phys.Rev. **C83**, 031901 (2011), arXiv:1011.6328 [nucl-ex].
- [9] P. Bozek, M. Chojnacki, W. Florkowski, and B. Tomasik, Phys.Lett. **B694**, 238 (2010), arXiv:1007.2294 [nucl-th].
- [10] T. Hirano, P. Huovinen, and Y. Nara, Phys.Rev. **C83**, 021902 (2011), arXiv:1010.6222 [nucl-th].
- [11] B. Schenke, S. Jeon, and C. Gale, Phys.Rev.Lett. **106**, 042301 (2011), arXiv:1009.3244 [hep-ph]; Phys.Lett. **B702**, 59 (2011), arXiv:1102.0575 [hep-ph].
- [12] H. Song, S. A. Bass, and U. Heinz, Phys.Rev. **C83**, 054912 (2011), arXiv:1103.2380 [nucl-th]; C. Shen, U. Heinz, P. Huovinen, and H. Song, Phys.Rev. **C82**, 054904 (2010), arXiv:1010.1856 [nucl-th]; F. G. Gardim, F. Grassi, M. Luzum, and J.-Y. Ollitrault, Phys.Rev.Lett. **109**, 202302 (2012), arXiv:1203.2882 [nucl-th].
- [13] H. Niemi, G. Denicol, P. Huovinen, E. Molnar, and D. Rischke, Phys.Rev. **C86**, 014909 (2012), arXiv:1203.2452 [nucl-th].
- [14] G.-Y. Qin, H. Petersen, S. A. Bass, and B. Muller, Phys.Rev. **C82**, 064903 (2010), arXiv:1009.1847 [nucl-th].
- [15] J.-Y. Ollitrault, Phys. Rev. **D46**, 229 (1992).
- [16] A. Adare et al. (PHENIX), Phys. Rev. Lett. **105**, 062301 (2010), arXiv:1003.5586 [nucl-ex].
- [17] R. Lacey (PHENIX Collaboration), J.Phys. **G38**, 124048 (2011), arXiv:1108.0457 [nucl-ex].
- [18] A. Adare et al. (PHENIX Collaboration), Phys.Rev.Lett. **107**, 252301 (2011), arXiv:1105.3928 [nucl-ex]; K. Aamodt et al. (ALICE Collaboration), Phys.Rev.Lett. **107**, 032301 (2011), arXiv:1105.3865 [nucl-ex]; G. Aad et al. (ATLAS Collaboration), Phys.Rev. **C86**, 014907 (2012), arXiv:1203.3087 [hep-ex]; P. Sorensen (STAR Collaboration), J.Phys. **G38**, 124029 (2011), arXiv:1110.0737 [nucl-ex]; S. Sanders (CMS Collaboration), PoS **QNP2012**, 148 (2012).
- [19] P. Kovtun, D. Son, and A. Starinets, Phys.Rev.Lett. **94**, 111601 (2005), arXiv:hep-th/0405231 [hep-th].
- [20] T. Hirano, U. W. Heinz, D. Kharzeev, R. Lacey, and Y. Nara, Phys.Lett. **B636**, 299 (2006), arXiv:nucl-th/0511046 [nucl-th].
- [21] H.-J. Drescher, A. Dumitru, A. Hayashigaki, and Y. Nara, Phys.Rev. **C74**, 044905 (2006), arXiv:nucl-th/0605012 [nucl-th]; H.-J. Drescher and Y. Nara, Phys.Rev. **C76**, 041903 (2007), arXiv:0707.0249 [nucl-th]; Z. Qiu and U. W. Heinz, Phys.Rev. **C84**, 024911 (2011), arXiv:1104.0650 [nucl-th].
- [22] B. Schenke, P. Tribedy, and R. Venugopalan, Phys.Rev.Lett. **108**, 252301 (2012),

- 382 arXiv:1202.6646 [nucl-th].
- 383 [23] R. A. Lacey, R. Wei, N. Ajitanand, and  
 384 A. Taranenko, Phys.Rev. **C83**, 044902 (2011),  
 385 arXiv:1009.5230 [nucl-ex]; R. Snellings,  
 386 J.Phys. **G38**, 124013 (2011), arXiv:1106.6284 [nucl-ex].
- 387 [24] C. Shen, S. A. Bass, T. Hirano, P. Huovi-  
 388 nen, Z. Qiu, et al., J.Phys. **G38**, 124045 (2011),  
 389 arXiv:1106.6350 [nucl-th]; Z. Qiu and  
 390 U. Heinz, AIP Conf.Proc. **1441**, 774 (2012),  
 391 arXiv:1108.1714 [nucl-th].
- 392 [25] R. A. Lacey, Y. Gu, X. Gong, D. Reynolds, N. Ajitanand,  
 393 et al., (2013), arXiv:1301.0165 [nucl-ex].
- 394 [26] R. A. Lacey, A. Taranenko, N. Ajitanand, and J. Alexan-  
 395 der, (2011), arXiv:1105.3782 [nucl-ex].
- 396 [27] R. A. Lacey, A. Taranenko, J. Jia, D. Reynolds, N. Aji-  
 397 tanand, et al., (2013), arXiv:1305.3341 [nucl-ex].
- 398 [28] E. Shuryak and I. Zahed, (2013),  
 399 arXiv:1301.4470 [hep-ph].
- 400 [29] J. Schukraft, A. Timmins, and S. A. Voloshin,  
 401 Phys.Lett. **B719**, 394 (2013), arXiv:1208.4563 [nucl-ex].
- 402 [30] H. Song, S. A. Bass, U. Heinz, T. Hirano,  
 403 and C. Shen, Phys.Rev. **C83**, 054910 (2011),  
 404 arXiv:1101.4638 [nucl-th]; See Fig. 14 in CMS PAS  
 405 HIN-12-011.
- 406 [31] A. Dobrin (ALICE Collaboration),  
 407 Nucl.Phys. **A904-905**, 455c (2013),  
 408 arXiv:1211.5348 [nucl-ex].
- 409 [32] S. Chatrchyan et al. (CMS Collabo-  
 410 ration), Phys.Rev. **C87**, 014902 (2013),  
 411 arXiv:1204.1409 [nucl-ex].
- 412 [33] J. Adams et al. (STAR Collabora-  
 413 tion), Phys.Rev. **C72**, 014904 (2005),  
 414 arXiv:nucl-ex/0409033 [nucl-ex].
- 415 [34] M. L. Miller, K. Reygers, S. J. Sanders, and P. Steinberg,  
 416 Ann. Rev. Nucl. Part. Sci. **57**, 205 (2007); B. Alver  
 417 et al., Phys. Rev. Lett. **98**, 242302 (2007).
- 418 [35] D. Kharzeev and M. Nardi,  
 419 Phys.Lett. **B507**, 121 (2001),  
 420 arXiv:nucl-th/0012025 [nucl-th].
- 421 [36] T. Lappi and R. Venugopalan,  
 422 Phys. Rev. **C74**, 054905 (2006); B. Schenke,  
 423 S. Jeon, and C. Gale, Phys.Rev. **C85**, 024901 (2012),  
 424 arXiv:1109.6289 [hep-ph].
- 425 [37] C. Gale, S. Jeon, B. Schenke, P. Tribedy, and R. Venu-  
 426 gopalan, (2012), arXiv:1210.5144 [hep-ph].
- 427 [38] Z. Qiu, C. Shen, and U. Heinz,  
 428 Phys.Lett. **B707**, 151 (2012), arXiv:1110.3033 [nucl-th].